SATELLITE IMAGERY CLASSIFICATION WITH LIDAR DATA

M. C. Alonso *, J. A. Malpica

School of Geodesy and Cartography, University of Alcalá, Ap. Correos 20, 28871 Alcalá de Henares, Madrid, Spain – (mconcepcion.alonso, josea.malpica)@uah.es

Commission VIII, WG 8

KEY WORDS: LIDAR, Satellite Imagery, Classification, Support Vector Machine, Feature Extraction, SPOT5

ABSTRACT:

This paper shows the potential of LIDAR for extracting buildings and other objects from medium resolution satellite imagery. To that end, the study integrated multispectral and LIDAR elevation data in a single imagery file and then classified it using the Support Vector Machine. To determine the method's potential, the study used a SPOT5 satellite from an area situated southeast of Madrid, Spain. First, with the four multispectral bands and the panchromatic band of the SPOT5 image, a multispectral four bands pansharpening was performed with Principal Component Analysis. Once integrated, these four pansharpening images and LIDAR data, were treated as independent multiple band imagery to perform the classification.
Using five classes, a sample of ground truth pixels was taken for training and testing. The study used 10% of the ground truth for training and the entire ground truth for testing the robustness of the classification with and without LIDAR data. To assess and compare the classification results numerically, confusion matrices and Receiver Operating Characteristic (ROC) were calculated for the five classes, for both classifications, with and without LIDAR.
Generally, when using only multispectral imagery, some confusion among classes occurs; for instance, buildings with flat asphalt roofs represent a separate problem in classification, since they are extremely difficult to discern from roads. This is mostly solved when integrating LIDAR data to the multispectral imagery. In general, when adding LIDAR, the classification results show a more realistic and homogeneous distribution of geographic features than those obtained when using multispectral SPOT5 alone.

1. INTRODUCTION

The automatic extraction of buildings and vegetation in urban areas can be used when updating urban inventories to monitor post-disaster emergencies and to assess building or vegetation changes. Regardless of the hazard's origin, post-disaster emergency agencies need to assess the geographic extent of the damage caused by the disaster and prioritize areas that need urgent assistance. Remote sensing techniques can perform some damage assessment tasks; the data obtained from remote sensing can be integrated into a Geographic Information System and consequently enhance the effectiveness and efficiency of emergency management.

Currently, operators manually extract cartographic features, such as buildings, roads, and trees, by visual interpretation of satellite imagery and aerial photography. Semi-automatic algorithms to assist cartographic technicians would improve the process. Common classification algorithms for low-resolution satellite imagery are too limited to deal with complex high-resolution satellite data and require new algorithms. Several authors have studied classification methods for satellite images (Bernardini et al., 2008; Alonso et al., 2007).

The combination of LIDAR (Light Detection and Ranging) with multispectral imagery can significantly improve classification, both in terms of accuracy and automation. LIDAR provides the altitude necessary for discriminating between certain classes but is blind to the type of object it measures, while the multispectral data provides intensity and facilitates the identification of the type of object. In this paper, we show the benefits of synergistically merging sensors for mapping buildings. The automatic extraction of buildings and vegetation in urban areas can aid in the important application of updating urban inventories to monitor urban vegetation and to assess buildings or vegetation changes.

Several authors have combined multispectral and LIDAR data. Syed et al. (2005) consider object-oriented classification as superior to maximum likelihood in terms of reducing "salt and pepper." Alia et al. (2008) describe an automated procedure for identifying forest species at the tree level from high-resolution imagery and LIDAR data. The results show an improvement in the ability to discriminate between tree classes. Zeng et al. (2002) showed an improvement in the classification of Ikonos imagery when integrated with LIDAR. This integration of LIDAR with multispectral data has proven beneficial for: the detection of buildings (Rottensteiner et al., 2003); the facilitation of accurate delineation of impervious surfaces (Hung and Germaine, 2008); change detection and quality control in urban areas (Walter, 2005); the extraction of roads (Hu et al., 2004); and the classification of coastal areas (Lee and Shan, 2003). The integration of multispectral imagery and multi-return LIDAR for estimating attributes of trees was reported in Collins et al. (2004). Our work combines LIDAR elevation data and SPOT5 multispectral data for the classification of urban areas. We used the Support Vector Machine (SVM), and our results confirm those of the above works by providing additional data and classification algorithm.

* Corresponding author.

2. MATERIALS AND STUDY AREA

SPOT5 satellite imagery has been used to determine the method's potential. Launched in 2002, this satellite captures panchromatic images with a 2.5 m resolution and multispectral images with a 10 m resolution (for the bands R, G, and NIR), and 20 m (for the MIR band). This experiment captured the scene at 11:20 a.m. on 12 August 2006; it represents an urban area southeast of Madrid, Spain, on mostly flat terrain. Figure 1 (a) shows the study area in a false color SPOT image generated with bands 1, 2, and 3 for the RGB monitor channels.

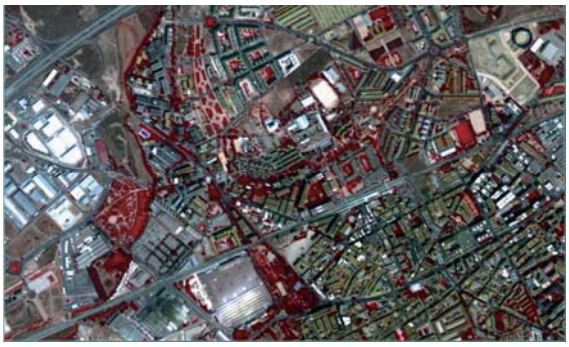

(a)

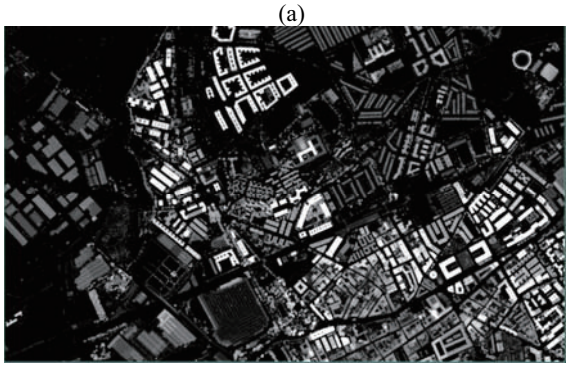

(b)

Figure 1. False color SPOT image (© SPOT Image Copyright 2004) (a) and LIDAR elevation data (b)

An aerial flight for the same area described for the SPOT5 scene took place also in August 2006 for the acquisition of LIDAR data. We obtained the density of the LIDAR with an average of three points per square meter, subtracted the Digital Terrain Model from the Digital Surface Model, and created the elevation model shown in Figure 1 (b). As mentioned earlier, this shows the LIDAR elevation image of the same area as Figure 1 (a).

The algorithm used for the classification was the Support Vector Machine (SVM); a detailed description of this algorithm can be found in Vapmik (1995). The idea for SVM initially appeared in an article by Boser et al. (1992), in which they applied it to optical character recognition problems. The authors demonstrated the superior generalization of SVM as compared with other learning algorithms. SVM maximizes the margin between the training patterns and the decision boundary.

Several authors have applied SVM to images; for instance, Azimi-Sadjadi and Zekavat (2000) used SVM to classify 10 different cloud and cloudless areas. The SVM has been compared to other classification methods for remote sensing imagery such as Neural Networks, Nearest Neighbor, Maximum Likelihood and Decision Tree classifiers, surpassing them all in robustness and accuracy (Huang et al., 2002; Foody and Mathur, 2004; Melgani and Bruzzone, 2004; Theodoridis and Koutroumbas, 2003; Perkins et al., 2001). These works led us to apply SVM rather than other methods for classification.

3. CLASSIFICATION OF SPOT5 WITH LIDAR

With the four multispectral bands and the panchromatic image, we carried out a multispectral four bands pansharpening performed with PCA (Figure 2).

The SPOT5 multispectral pansharpening images and the LIDAR data are integrated and treated as independent multiple band imagery to carry out the classification.

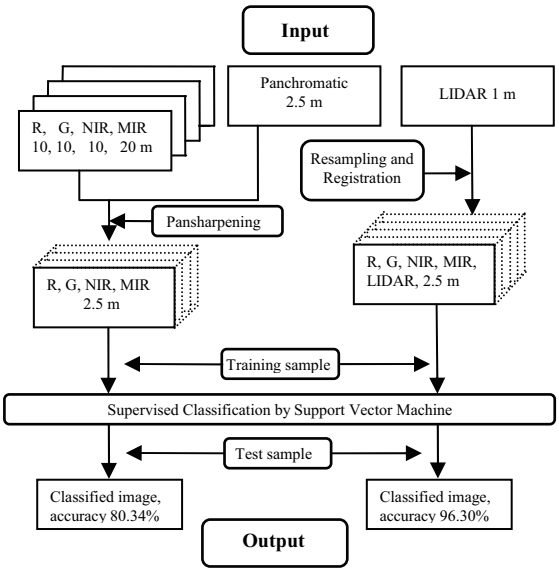

Figure 2. Flow chart for the classification

This study tested several provisional numbers of classes and training samples for the SVM classifier and performed quality assessment following the methodology described in Alonso et al. (2008). Eventually, we established an arrangement of five classes: high vegetation (trees, A), low vegetation (shrubs and lawns, B), natural grounds (C), artificial grounds (D), and buildings (E). With the help of aerial photos and ground visits, we selected samples for training and evaluating the classifier from the SPOT–LIDAR merged data set. The study area corresponded to the city of Alcalá de Henares where the authors reside and allowed for many visits and opportunities for gathering samples. Finally, a ground truth of 11020 pixels was selected. Table 1 and Figure 3 show the distribution of the ground truth.

For training we took a 10% random subset of the ground truth sample. However, we carried out the test with the whole ground truth.

	Ground truth sample	
	Pixels	Percent
Trees (A)	2106	19,11
Shrubs and lawns (B)	982	8,91
Natural grounds (C)	2310	20,96
Artificial grounds (D)	2284	20,73
Buildings. (E)	3338	30,29
Total	11020	100

Table 1. Class Distribution Summary

Figure 3. Distribution of the ground truth

4. RESULTS AND DISCUSSION

Figure 4 (a) shows the results for the classification of the multispectral image plus LIDAR data, while Figure 4 (b) shows the classification without LIDAR. A simple visual analysis of both images reveals the superior delineation of cartographic features in Figure 4 (a) over those of Figure 4 (b).

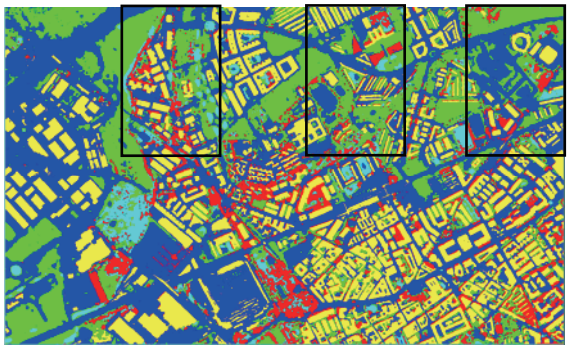

(a)

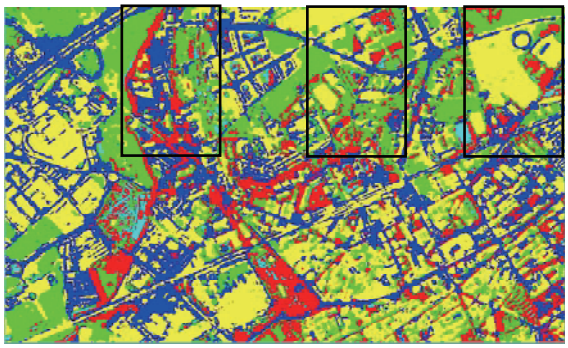

(b)

Figure 4. Results of the SVM classifications with LIDAR (a) and without LIDAR (b)

Figures 5 (a), 6 (a), and 7 (a) show three aerial images representing three details from Figure 4 (a) and Figure 4 (b), represented with rectangles in Figure 4. Figures 5 (b), 6 (b), and 7 (b) show the classifications of the three details using multispectral bands plus LIDAR. Figures 5 (c), 6 (c), and 7 (c) represent the classifications of multispectral bands without adding LIDAR.

The left upper corner of Figure 5 (a) shows a motorway correctly detected in Figure 5 (b) but not in Figure 5 (c), where it has been confused with the buildings class. Obviously, the LIDAR data has discriminated the motorway as ground by the SVM when classifying with multispectral imagery adding LIDAR. On the contrary, in the central part of Figure 5 (a) we can see several buildings detected in Figure 5 (b) while in Figure 5 (c), these same buildings have been wrongly taken for artificial ground. Furthermore, the buildings detected in Figure 5 (c) are fuzzier than those in Figure 5 (b); again, the LIDAR data has allowed sharper discrimination by considering height. Visits to the terrain prove that the classification in Figure 5 (b) distinguishes the trees class from the shrubs and lawn class better than the classification in Figure 5 (c). For instance, note the red diagonal of Figure 5 (c) and the cross form at the middle left side of the image to the middle upper side. See Figure 5 (b) and the roundabout at the upper right corner. Figure 5 (b) correctly detects shrubs and lawn (with two trees taken also correctly by two of the red points), while 5 (c) has wrongly mistaken the objects as mostly trees.

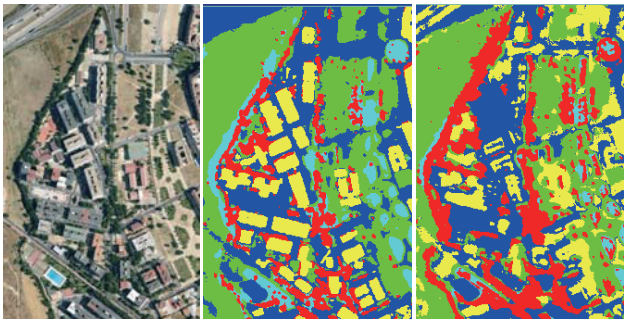

(a) (b) (c)

Figure 5. Aerial image for reference (a), results of SVM classifications with LIDAR (b), and without LIDAR (c)

The upper part of Figure 6 (a) shows several semi-attached buildings correctly detected in Figure 6 (b), while they are mistaken as a unique building in Figure 6 (c). Also, Figure 6 (b) has correctly classified the parking lots as artificial ground (blue color), while Figure 6 (c) has mistaken them as buildings.

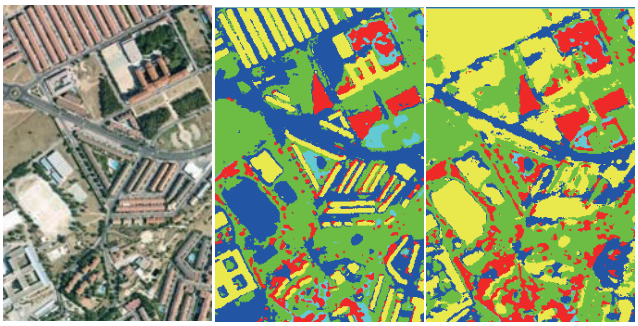

(a) (b) (c)

Figure 6. Aerial image for reference (a), results of SVM classifications with LIDAR (b), and without LIDAR (c)

Figure 7 (a) reveals a bullfighting arena (the round object toward the top of the figure). Figure 7 (b) correctly classifies it as a building, while it has been mistaken as artificial ground in Figure 7 (c). The surroundings of the bullfighting arena corresponding to parking lots have been detected correctly as artificial ground in Figure 7 (b) and wrongly classified as buildings in Figure 7 (c).

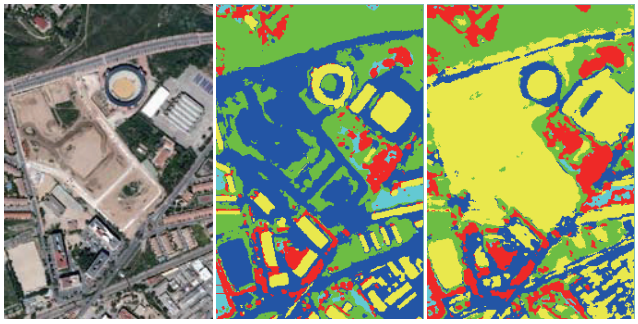

(a) (b) (c)

Figure 7. Aerial image for reference (a), results of SVM classifications with LIDAR (b), and without LIDAR (c)

To assess and compare the classification results numerically, we calculated confusion matrices for both classifications, with and without LIDAR. Table 2 shows the confusion matrix for the classification of Figure 4 (a), while Table 3 shows the confusion matrix corresponding to Figure 4 (b).

Ground Truth / Class (Pixels)	A	B	C	D	E	Total
Trees (A)	2091	0	0	15	0	2106
Shrubs (B)	0	958	0	6	0	964
Natur. g(C)	0	3	2310	39	0	2352
Artif. g (D)	0	21	0	2115	109	2245
Build. (E)	15	0	0	109	3229	3353
Total	2106	982	2310	2284	3338	11020

Table 2. Confusion matrix for classification with the LIDAR band.

Overall Accuracy = (10703/11020) ~ 97.1234% and Kappa Coefficient = 0.9630

Ground Truth / Class (Pixels)	A	B	C	D	E	Total
Trees (A)	2010	78	0	23	2	2113
Shrubs (B)	79	878	0	2	0	959
Natur. g(C)	17	1	2225	104	166	2513
Artif. g (D)	0	25	0	1057	486	1568
Build. (E)	0	0	85	1098	2684	3867
Total	2106	982	2310	2284	3338	11020

Table 3. Confusion matrix for classification without LIDAR

Overall Accuracy = (8854/11020) ~ 80.3448% and Kappa Coefficient = 0.7454

The overall accuracy and the Kappa coefficients are 97.12% and 0.96 (see Table 2) for the SVM classification with LIDAR data, shown in Figure 4 (a), while overall accuracy reaches 80.34% and 0.7454 (see Table 3) for the SVM classification without LIDAR data, as shown in Figure 4 (b). Therefore, a gain of 16.77% is obtained in merging the LIDAR data with the multispectral bands for this data set. The confusion matrices allow us to examine the differences of the classifications in detail. For all the classes considered, the omission and commission errors are improved to some degree by the integration of LIDAR (see Table 4).

Per cent	With LIDAR		Without LIDAR	
	Omission	Commission	Omission	Commission
Trees (A)	0.71	0.71	4.56	4.87
Shrubs (B)	2.44	0.62	10.59	8.45
Natur.(C)	0.00	1.79	3.68	11.46
Artif. (D)	7.40	5.79	53.72	32.59
Build. (E)	**3.27**	**3.70**	**19.59**	**30.59**

Table 4. Classification errors for with and without LIDAR

Table 4 shows the buildings class with an omission error of 19.59% and a commission error of 30.59% without LIDAR, whereas the addition of LIDAR reduces these errors to 3.27% and 3.70%, respectively. This is a consequence of introducing elevation data, which allows building extraction to take place more accurately, as seen in the comparison between the classifications presented in Figure 4 (a and b). To a lesser degree than with the buildings, we can observe an improvement in the classification of vegetated areas between high vegetation (trees) and low vegetation (lawns, grass, or shrubs).

Spectral signatures of some urban materials are similar in composition. For instance, the roofs of some buildings and roads and parking lots are made of asphalt, therefore the multispectral classifier (without LIDAR) assigns them to the same class; however, when we consider LIDAR elevation data, the classifier discriminates between buildings and artificial grounds, and these errors disappear.

As a measure of performance of supervised classification, we use the receiver operating characteristic (ROC) curve (see Figure 8). See also Metz (1978), for additional information.

Many applications use the area under the ROC curve (AUROC) as a measure of accuracy (Hanley and McNeil, 1982). For the five classes considered in this work, the AUROCs are bigger using LIDAR than without it (Table 5).

Area under the ROC curve	LIDAR	
	With	Without
Trees (A)	0.97784	0.94885
Shrubs and lawns (B)	0.99475	0.99405
Natural grounds (C)	0.93395	0.90910
Artificial grounds (D)	0.82263	0.71577
Buildings. (E)	0.90492	0.80629

Table 5. Area under the ROC curve for each class with LIDAR and without LIDAR classification

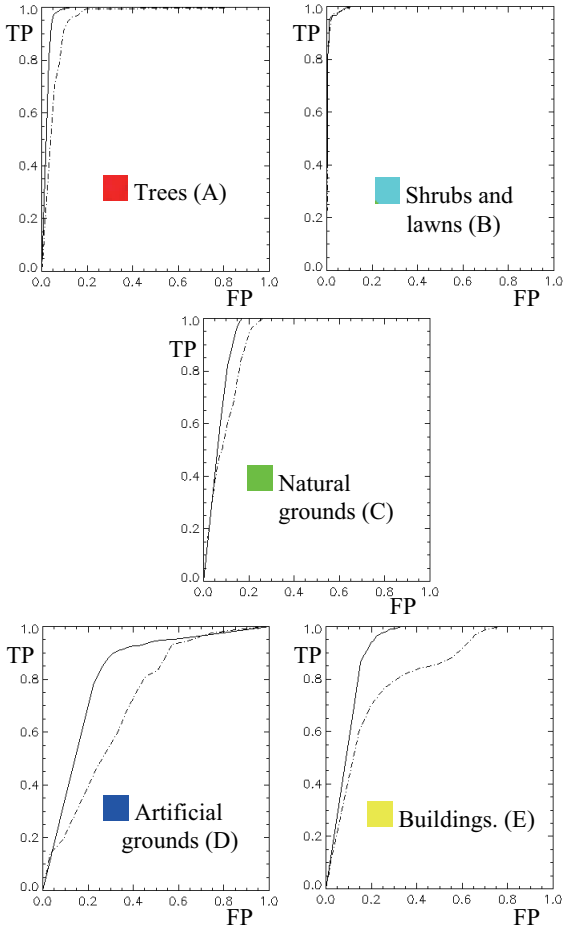

Figure 8. ROC curves in the SVM classifications with (straight line) and without (dotted line) LIDAR. TP and FP are true positive and false positive

5. CONCLUSIONS

This study investigated the impact of LIDAR data on the classification of multispectral SPOT5 imagery using SVM over an urban area near Madrid, Spain. A visual evaluation shows an improvement of the classification when using LIDAR data. Two numerical methods—confusion matrices and ROC curves—complemented this evaluation of the results. After defining ground truth samples, we used 10% randomly for training for both classifications (with and without LIDAR), while the evaluation was made with the total ground truth samples. We obtained a gain of 16.78% in overall accuracy for the imagery in this experiment. Furthermore, ROC curves for the classification with LIDAR reveal a superior performance for all classes compared to the classifications without it.

The SVM classifier with LIDAR shows a more realistic and homogeneous distribution of geographic features than that obtained without LIDAR. This is specifically so for buildings and artificial ground, as shown by the ROC curves.

REFERENCES

Alia, S.S., Dareb, P., Jonesc, S.D., 2008. Fusion of remotely sensed multispectral imagery and Lidar data for forest structure assessment at the tree level. In: *The International Archives of the Photogrammetry, Remote Sensing and Spatial Information Sciences,* Beijing, Vol. XXXVII. Part B7, pp 1089-1094.

Alonso, M.C. and Malpica, J.A, 2008. Classification of Multispectral High-Resolution Satellite Imagery Using LIDAR Elevation Data. In Bebis G. et al. (Eds.): *Advances in Visual Computing ISVC08,* Part II, Lecture Notes in Computer Science 5359, pp. 85–94. Springer-Verlag.

Alonso, M.C., Sanz, A. and Malpica, J.A., 2007. Classification of high resolution satellite images using texture. In Bebis G. et al. (Eds.): *Advances in Visual Computing ISVC07.* Part II LNCS 4842, pp. 499–508. Springer-Verlag.

Azimi-Sadjadi, M.R. and Zekavat, S.A., 2000. Cloud classification using support vector machines. In: *Proceedings of the 2000 IEEE Geoscience and Remote Sensing Symposium IGARS*, Vol. 2, pp. 669 – 671.

Bernardini, A., Malinverni, E. S., Zingaretti, P. and Mancini, A., 2008. Automatic classification methods of high-resolution satellite images: the principal component analysis applied to the sample training set. In: *The International Archives of the Photogrammetry, Remote Sensing and Spatial Information Sciences,* Beijing, Vol. XXXVII. Part B7, pp 701-706.

Boser, B.E., Guyon, I. and Vapnik, V.N., 1992. A Training Algorithm for Optimal Margin Classifiers. In: D. Haussler, editor, *Proceedings of the Fifth Annual Workshop on Computational Learning Theory* pp. 144-152, Pittsburgh. ACM Press.

Collins, C.A., Parker, R.C. and Evans, D.L., 2004. Using multispectral imagery and multi-return LIDAR to estimate trees and stand attributes in a southern bottomland Hardwood forest. In: *ASPRS Annual Conference Proceedings,* Denver, Colorado (on CD-ROM).

Foody, G.M. and Mathur, A., 2004. A Relative Evaluation of Multiclass Image Classification by Support Vector Machines. In: *IEEE Transactions On Geoscience And Remote Sensing*, Vol. 42(6), pp. 1335-1343.

Hanley, J.A. and McNeil, B.J., 1982. The Meaning and Use of the Area under a Receiver Operating Characteristic (ROC) Curve. *Radiology,* Vol. 143, pp. 29-36.

Hu, X., Tao C.V. and Hu, Y, 2004. Automatic road extraction from dense urban area by integrated processing of high resolution imagery and lidar data. In: *International Society for Photogrammetry and Remote Sensing (ISPRS),* Istanbul, Turkey.

Huang, C., Davis, L.S. and Townshed, J.R.G., 2002. An assessment of support vector machines for land cover classification. *International Journal of Remote Sensing,* Vol. 23, pp. 725–749.

Hung, M.C. and Germaine, K., 2008. Delineating Impervious Surfaces Utilizing High Spatial Resolution Multispectral

Imagery and Lidar Data. In: *ASPRS 2008 Annual Conference,* Portland, Oregon.

Lee, D.S. and Shan, J., 2003. Combining Lidar Elevation Data and IKONOS Multispectral Imagery for Coastal Classification Mapping. *Marine Geodesy, an International Journal of Ocean Surveys, Mapping and Remote Sensing*, Vol. 26(1-2), pp.117-127.

Melgani, F. and Bruzzone, L., 2004. Classification of Hyperspectral Remote Sensing Images With Support Vector Machines. In: *IEEE Transactions On Geoscience And Remote Sensing*, Vol. 42(8), pp. 1778–1790.

Metz, C.E., 1978. Basic principles of ROC analysis. *Seminars Nuclear Medicine,* Vol. 8(4), pp. 283-298.

Perkins, S., Harvey, N.R., Brumby, S.P. and Lacker, K. 2001. Support Vector Machines for broad area feature classification in remotely sensed images. In: *Proceeding of Algorithms for multispectral, hyperstral, and ultraspectral imagery,* Vol. 4381, pp. 286-295, Orlando USA.

Rottensteiner, F., Trinder, J., Clode S. and Kubic, K., 2003. Building dectection using LIDAR data and multispectral images. In: *Proceedings of DICTA,* Sydney, Australia, pp. 673–682.

Syed, S., Dare, P. and Jones, S., 2005. Automatic classification of land cover features with high resolution imagery and Lidar data: an objectoriented approach. *Proceedings of SSC2005 Spatial Intelligence, Innovation and Praxis: The national biennial Conference of the Spatial Sciences Institute,* Melbourne, Australia, Sep.

Theodoridis, S. and Koutroumbas, K., 2003. *Pattern Recognition*. Second Edition. Elsevier Academic Press.

Vapmik, V., 1995. *The Nature of Statistical Learning Theory*. Springer Verlag. New York.

Walter, V., 2005. Object-based classification of integrated multispectral and LIDAR data for change detection and quality control in urban areas. In: *Proceedings of the ISPRS WG VII/1Human Settlements and Impact Analysis*.

Zeng, Y., Zhang, J., Wang, G. and Lin, Z., 2002. Urban landuse classification using integrated airborn laser scanning data and high resolution multispectral imagery, Pecora 15/Land Satellite Information IV/ISPRS Commssion I/FIEOS.

ACKNOWLEDGEMENTS

The authors wish to thank the Spanish National Mapping Agency (Instituto Geográfico Nacional) for providing the images and LIDAR data for this research. The authors are also grateful to the Spanish MICINN for financial support to present this paper in ISPRS; project number CGL2009-13768.